

1 **Quantitative Mapping of Collagen Fiber Orientation in Non-Glaucoma and**  
2 **Glaucoma Posterior Human Scleras**

3 *Jacek K. Pijanka<sup>1</sup>, Baptiste Coudrillier<sup>2</sup>, Kimberly Ziegler<sup>2</sup>, Thomas Sorensen<sup>3</sup>, Keith*  
4 *M. Meek<sup>1</sup>, Thao D. Nguyen<sup>2</sup>, Harry A. Quigley<sup>4</sup>, Craig Boote<sup>1</sup>*

5 <sup>1</sup> Structural Biophysics Group, School of Optometry and Vision Sciences, Cardiff  
6 University, Cardiff, UK.

7 <sup>2</sup> Department of Mechanical Engineering, Johns Hopkins University, Baltimore, USA.

8 <sup>3</sup> Diamond Light Source, Didcot, UK.

9 <sup>4</sup> Glaucoma Center of Excellence, Wilmer Ophthalmological Institute, Johns Hopkins  
10 University School of Medicine, Baltimore, USA.

11

12 Short Title: Fiber orientation in posterior human sclera

13 Section Code: GL

14 Word count (text): 4,875

15 Figures: 8 (+ 3 supplementary)

16 Tables: 2

17

18 Keywords: sclera, collagen, x-ray scattering, multiphoton microscopy, glaucoma

19

20 Commercial Relationship Policy: N

21 Funding: Fight for Sight Grant 1360, NIH Grants EY021500, EY02120 and EY01765,

22 USAMRMC Award W81XWH-10-1-0766.

23 This work was presented in part at the ARVO annual meeting, May 2010.

1 Corresponding Author:  
2 Craig Boote,  
3 Structural Biophysics Group,  
4 School of Optometry and Vision Sciences,  
5 Cardiff University,  
6 Maindy Road,  
7 Cardiff CF24 4LU,  
8 UK.  
9 Tel: +44 (0)2920 870586  
10 Fax: +44 (0)2920 874859  
11 Email: [bootec@cf.ac.uk](mailto:bootec@cf.ac.uk)

12

13

14

15

16

17

18

19

20

21

22

23

## 1 **ABSTRACT**

2 **Purpose:** The posterior sclera has a major biomechanical influence on the optic nerve  
3 head, and may therefore be important in glaucoma. Scleral material properties are  
4 influenced significantly by collagen fiber architecture. Here we quantitatively map fiber  
5 orientation in non-glaucoma and glaucoma posterior human scleras.

6 **Methods:** Wide-angle x-ray scattering quantified fiber orientation at 0.5mm intervals  
7 across 7 non-glaucoma post-mortem human scleras, and 5 scleras with glaucoma history  
8 and confirmed axon loss. Multiphoton microscopy provided semi-quantitative depth-  
9 profiling in the peripapillary sclera.

10 **Results:** Mid-posterior fiber orientation was either uniaxial (one preferred direction) or  
11 biaxial (two directions). The peripapillary sclera was characterized by a ring of fibers  
12 located mainly in the mid/outer stromal depth and encompassing ~50% of the total  
13 tissue thickness. Fiber anisotropy was 37% higher in the peripapillary sclera compared  
14 to mid-posterior, varied up to four-fold with position around the scleral canal, and was  
15 consistently lowest in the superior-nasal quadrant. Mean fiber anisotropy was  
16 significantly lower in the superior-temporal ( $p < 0.01$ ) and inferior-nasal ( $p < 0.05$ )  
17 peripapillary scleral quadrants in glaucoma compared to non-glaucoma eyes.

18 **Conclusions:** The collagen fiber architecture of the posterior human sclera is highly  
19 anisotropic and inhomogeneous. Regional differences in peripapillary fiber anisotropy  
20 between non-glaucoma and glaucoma eyes may represent adaptive changes in response  
21 to elevated IOP and/or glaucoma, or baseline structural properties that associate with  
22 predisposition to glaucomatous axon damage. Quantitative fiber orientation data will

1 benefit numerical eye models aimed at predicting the sclera's influence on nerve head  
2 biomechanics, and thereby its possible role in glaucoma.

3

4

5

6

7

8

9

10

11

12

13

14

15

16

17

18

19

20

21

22

23

24

## 1 **INTRODUCTION**

2           The sclera forms approximately 85% of the eye's outer tunic in humans,  
3 providing a tough, fibrous supporting substrate for the other ocular components  
4 including the retina and optic nerve head. A complex network of collagen fibers forms  
5 the sclera's major load-carrying component<sup>1</sup>, and is a major influence on the tissue's  
6 biomechanical response to changes in intraocular pressure (IOP)<sup>2</sup>. Accurate,  
7 quantitative information on scleral fiber architecture will therefore be important in order  
8 to understand and model the tissue's physiological load-bearing behaviour and its  
9 clinical implications.

10           In the biomechanical paradigm of glaucoma, it is proposed that IOP-induced  
11 deformation in and around the lamina cribrosa initiates a complex cascade of events that  
12 ultimately result in ganglion cell dysfunction and apoptosis<sup>3, 4</sup>. The physical effects of  
13 IOP on nerve axons as they traverse the lamina are transmitted both directly via the  
14 trans-lamina pressure differential, and also indirectly via the supporting tissues of the  
15 eye-wall, of which the sclera is paramount as the main stress-bearing tissue<sup>2, 5-8</sup>. While  
16 the properties of the lamina itself, as the main injury site<sup>9</sup>, are important in glaucoma,  
17 recent research suggests that the mechanical influence of the surrounding sclera may  
18 also be key. Modelling studies have indicated that scleral shape, thickness and material  
19 properties are all influential factors<sup>5-7, 10</sup>, and that posterior scleral stiffness is a major  
20 material determinant of IOP-derived lamina strain<sup>7</sup>. In addition, alterations in tissue  
21 thickness<sup>11</sup>, mechanics<sup>12, 13</sup> and matrix ultrastructure<sup>14, 15</sup> in human and experimental  
22 glaucoma suggest a role for the peripapillary sclera in the disease mechanism.

23           A number of techniques have provided information on the arrangement of scleral  
24 collagen. Using histological reconstructions Kokott was the first to suggest, over 75

1 years ago, that the posterior scleral fibers adopt preferred orientations that may relate to  
2 physical forces acting on the globe<sup>16</sup>. A number of imaging tools have provided more  
3 recent insight, including transmission<sup>17</sup> and scanning<sup>18</sup> electron microscopy, atomic  
4 force microscopy<sup>18</sup> and second harmonic generation multiphoton microscopy<sup>19, 20</sup>.  
5 However these studies, while important, have provided largely qualitative and/or  
6 localised information. Most recently, small-angle light scattering has been used to  
7 quantify fiber orientation in rat sclera<sup>21</sup>. This method has also yielded valuable  
8 information on human tissue; albeit these measurements were restricted to the temporal  
9 region of the peripapillary sclera<sup>19</sup>. Thus extensive, quantitative information on collagen  
10 fiber orientation in the human sclera is still lacking in the literature.

11 We have developed a method, based on wide-angle-angle x-ray scattering  
12 (WAXS), which provides quantitative measurements of bulk collagen fiber orientation  
13 in situ, without the need for tissue processing that may perturb the native tissue  
14 structure. Previously we have applied this method to map fiber orientation in the cornea  
15 and the ~3mm of sclera adjacent to the limbus (reviewed<sup>22</sup>). However, up until now  
16 WAXS has not been employed in studies of the posterior sclera. In the current paper,  
17 our aim was to apply this technique to quantitatively map collagen fiber orientation in  
18 non-glaucoma and glaucoma posterior human scleras.

19

## 20 **METHODS**

### 21 **Tissue Details**

22 All experimental procedures were performed in accordance with the Declaration  
23 of Helsinki. Non-glaucoma and glaucoma human eyes, all from Caucasian donors, were  
24 obtained from the National Disease Research Interchange (NDRI) within 48 hours post-

1 mortem. Eyes were shipped on dry ice and preserved in balanced salt solution (BSS,  
2 Alcon, Inc., Fort Worth, TX). A provisional designation of glaucoma was made on the  
3 basis of either having an extensive history in the office of one of the authors (HAQ) pre-  
4 mortem (donor g1), or where post-mortem medical records showed a coded diagnosis of  
5 glaucoma by virtue of a documented prescription of known intraocular pressure  
6 lowering medications and/or where the family confirmed that the donor had been treated  
7 for glaucoma. Provisional non-glaucoma status was assigned where a specimen met  
8 none of these criteria. None of the eyes used in this study had any previous history of  
9 ocular surgery involving the posterior sclera.

10

### 11 **Specimen Preparation**

12       The surrounding fat, muscle and episcleral tissues were gently removed from  
13 each eye, and the optic nerve excised with a razor blade flush to the sclera and  
14 preserved in 4% paraformaldehyde (Electron Microscopy Sciences, Hatfield, PA) for  
15 subsequent axon loss grading. While keeping the intact eyes moist with BSS, the axial  
16 length and the nasal-temporal and superior-inferior globe diameters were measured  
17 using digital callipers. The cornea and anterior sclera were then excised and the lens,  
18 retina and choroid removed. The intact posterior scleras were stored in 4%  
19 paraformaldehyde at 4°C until the time of x-ray experiments. Our previous work has  
20 shown that this mild fixation method does not affect WAXS collagen orientation  
21 measurements<sup>23</sup>.

22

### 23 **Optic Nerve Grading**

1           To confirm the provisional glaucoma diagnosis, cross-sections were taken from  
2 each fixed optic nerve at locations 1-3 mm behind the eye, embedded in epoxy resin and  
3 sectioned at 1 $\mu$ m thickness. A glaucoma specialist (HAQ), experienced in optic nerve  
4 grading and masked to the provisional diagnosis, then assigned a quantitative grade  
5 from 0 to 3 for the degree of axon loss<sup>12,24</sup>, where: Grade 0 was < 10% loss (normal),  
6 Grade 1 was 10-25% loss (mild), Grade 2 was 25-50% loss (intermediate), Grade 3 was  
7 50-75% loss (severe). All non-glaucoma eyes were confirmed to have a grading of 0  
8 (normal), while only glaucoma eyes receiving a grading of 2 or 3 (intermediate/severe)  
9 were used in subsequent experiments. The resulting number of eyes available for  
10 WAXS was 7 non-glaucoma (from 6 donors) and 5 glaucoma (from 4 donors). The  
11 mean age of the non-glaucoma eyes was 76 ( $\pm$  7) yrs, and the mean age of the glaucoma  
12 eyes was 75 ( $\pm$  10) yrs. Details of all the eyes used are given in Table 1.

13

#### 14 **X-ray Scattering**

15           X-ray scattering experiments were carried out on Beamline I02 at the Diamond  
16 Light Source (Didcot), the UK's national synchrotron facility. Immediately prior to x-  
17 ray exposure, a 15mm circular specimen, centered on the optic nerve head, was excised  
18 from each intact fixed posterior sclera, wrapped in polyvinylidene chloride film to  
19 prevent tissue dehydration throughout the duration of the data collection (~1.5 hrs per  
20 specimen), and mounted inside Perspex® (Lucite Group Ltd, Southampton, UK)  
21 chambers with Mylar® (DuPont-Teijin, Middlesbrough, UK) windows. Each mounted  
22 specimen was oriented superior-side uppermost, its outer scleral surface towards the  
23 incident x-ray beam and with its natural curvature retained. WAXS patterns, each

1 resulting from an x-ray exposure of between 3s and 5s, were collected at 0.5mm  
2 (horizontal)  $\times$  0.5mm (vertical) intervals covering the whole of all but one specimen.  
3 The exception was non-glaucoma specimen n4r, for which an 11.5mm  $\times$  11.5mm raster  
4 scan was performed due to time limitations. WAXS patterns were recorded  
5 electronically on a CCD detector (ADSC, Poway, CA) placed 550mm behind the  
6 specimen position. Precise translation of the specimen between exposures was achieved  
7 using a motorized x-y stage interfaced with the x-ray camera shutter. The focussed x-ray  
8 beam had a wavelength of 0.09795nm and horizontal/vertical dimensions of 0.2mm.  
9 After WAXS experiments, each scleral specimen was immediately returned to 4%  
10 paraformaldehyde and stored at 4°C for subsequent multiphoton imaging.

11 The WAXS pattern from sclera is dominated by a well-resolved equatorial (i.e.  
12 perpendicular to the fiber axis) reflection from the regular 1.6nm spacing of the  
13 constituent collagen molecules aligned near-axially within the scleral fibers (Fig. 1A).  
14 Analysis of the angular spread of intensity around this reflection provides a quantitative  
15 measure of the relative number of fibers oriented at a given angle within the scleral  
16 plane, as an average value within the tissue volume traversed by the x-ray beam<sup>22</sup>. Thus  
17 the method can describe bulk collagen anisotropy in terms of the excess of fibers  
18 aligned in a given direction over and above the general population that are dispersed  
19 equally in all orientations.

20 The quantification of corneal and scleral collagen fiber orientation from WAXS  
21 patterns is described in detail elsewhere<sup>22</sup>. In brief, a two-dimensional background  
22 function was firstly fitted and subtracted from each WAXS pattern to remove scatter  
23 from the specimen chamber and all other tissue components other than fibrous collagen.

1 For every WAXS pattern, 256 equally spaced radial profiles from pattern center to  
2 beyond the collagen signal were generated and a unique power-law background  
3 function independently fitted to and subtracted from each (Fig. 1B), using a purpose-  
4 written Excel macro routine. The isolated collagen scatter peak for each of the 256  
5 angular directions was then normalised against fluctuations in x-ray beam current and  
6 exposure time, radially integrated, and the resulting values extracted to angular bins,  
7 using a combination of Optimas 6.5 (Media Cybernetics Inc., Marlow, UK) image  
8 analysis and Excel (Microsoft, Reading, UK) software. The resulting angular intensity  
9 profile (Fig. 1C) was divided into isotropic and anisotropic scatter components and the  
10 latter plotted in polar vector coordinates, introducing a  $90^\circ$  angular shift to account for  
11 equatorial scatter. Every sampled point in the sclera could thereby be represented by a  
12 polar vector plot (Fig. 1D), in which the length of a vector in any direction gave the  
13 relative number of fibers preferentially aligned in that direction, at that point in the  
14 tissue. Individual plots were then assimilated into montages showing the preferential  
15 fiber orientation across each specimen.

16 While the vector lengths within a given polar plot give an accurate measure of  
17 the relative fiber number for each angle at that point in the tissue, it should be noted that  
18 the relative overall size of individual plots between measurement points scales not only  
19 with the degree of preferential fiber alignment, but also with scleral thickness<sup>22</sup>. The  
20 scaling of the polar plots should therefore be only used as a qualitative guide to the level  
21 of collagen alignment. An accurate measure of the degree of fiber anisotropy in the  
22 tissue may be gained by computing the ratio of the preferentially aligned and total x-ray  
23 scatter to remove the thickness dependency<sup>22</sup>. This was done for every sampled point in  
24 the sclera by dividing the integral of the aligned scatter distribution (clear region in Fig.

1 1B) by the corresponding integral of the total scatter (clear plus shaded regions in Fig.  
2 1B), yielding a single value representing the proportion of fibers preferentially aligned  
3 at that point in the tissue. These values were then assimilated into Excel contour maps to  
4 show the variation in degree of fiber anisotropy across each specimen.

5 Scleral fiber anisotropy was statistically compared between the non-glaucoma  
6 and glaucoma groups. For each specimen, the 64 sampling points within a 1.5mm wide  
7 annulus adjacent to the scleral canal were considered as representing the peripapillary  
8 sclera (Fig. 2A). Over 98% of the polar vectors plots within this region indicated  
9 preferential fiber alignment circumferential to the scleral canal (Fig. 2B). All sampling  
10 points lying outside this region were considered mid-posterior sclera. The peripapillary  
11 and mid-posterior regions were then each sub-divided into their 4 principal quadrants  
12 (Fig. 2C) and the mean and variance of each sub-region was evaluated per specimen.  
13 Mid-posterior regional averages were not calculated for specimen n4r, due to this being  
14 a partial WAXS scan. Pooled anisotropy values within each of the 8 scleral regions  
15 were then compared for significant differences between non-glaucoma and glaucoma  
16 groups using Welch-corrected two-tailed t-test. To account for lower variability  
17 between eyes from the same donor, corresponding values within fellow eyes of the non-  
18 glaucoma (n1l and n1r) and glaucoma (g1l and g1r) pair were firstly averaged for  
19 subsequent statistical analysis.

20

## 21 **Multiphoton Microscopy**

22 Although WAXS provides highly quantitative measurements of bulk fiber  
23 anisotropy, it cannot tell us how individual fiber bundles are arranged within a given

1 scleral layer, nor how the orientation of fibers changes as a function of tissue depth.  
2 Multiphoton microscopy has been widely used to provide qualitative information of this  
3 kind from the sclera, including the peripapillary region<sup>19, 21</sup>. In order to determine the  
4 depth-dependency of fiber orientation in the peripapillary sclera of non-glaucoma and  
5 glaucoma eyes, multiphoton imaging was performed on two of the same non-glaucoma  
6 (n4r and n6r) and glaucoma (g1l and g3r) specimens previously examined by WAXS.  
7 Pilot experiments comparing tissue with and without x-ray exposure verified that  
8 WAXS did not result in any disruption or artefact in the resulting multiphoton collagen  
9 signal. Full-thickness circular specimens, centered on the optic nerve head, were excised  
10 from the fixed posterior scleral specimens using a 6mm biopsy punch. The resulting  
11 tissue pieces were then separated into six 150 $\mu$ m thick serial sections using a sledge  
12 microtome (HM440E, Microm, Walldorf, Germany), before being slide-mounted in 1:1  
13 PBS/glycerol for maintenance of tissue hydration and refractive index matching. A  
14 recent study showed that glycerol treatment does not significantly affect collagen fiber  
15 architecture<sup>21</sup>.

16 Non-linear laser-scanning multiphoton microscopy was performed using a  
17 commercial device (Zeiss LSM 510 META NLO, Carl Zeiss Ltd, Welwyn Garden City,  
18 UK). An Ultrafast titanium-sapphire laser (Cameleon, Coherent, Inc., UK) operating at  
19 800 nm and <140 fs/90 MHz pulses was used to produce second harmonic generation  
20 signals from fibrous collagen detected at  $400 \pm 10$  nm in the forward direction (non-  
21 descanned detector)<sup>25</sup>. A mid-depth image plane was obtained within each section using  
22 a Plan-Apochromat 20 $\times$ /0.8 N.A. objective lens, providing a 400 $\mu$ m  $\times$  400 $\mu$ m field-of-  
23 view. A 15  $\times$  15 field-of-view tiling, covering the whole of each section, was then

1 obtained using x-y motor stages (~1.5 hrs per section). The resulting datasets were  
2 reconstructed using Zeiss LSM Image Examiner 5.0 software.

3       Semi-quantitative depth profiles of fiber anisotropy in the peripapillary sclera  
4 were obtained from the multiphoton images at four separate locations in the  
5 peripapillary sclera, one per tissue quadrant. The fast Fourier transform (FFT)  
6 processing algorithm of ImageJ (W. Rasband, NIH, Bethesda, MD) was used to  
7 generate a theoretical diffraction pattern from each image (Fig. 3A, B). The baseline  
8 intensity for each FFT pattern was removed, the central 100 pixel radial zone integrated,  
9 and the azimuthal intensity distribution extracted to 256 equally spaced bins (Fig. 3B,  
10 C), using Fit2D diffraction analysis software (A. P. Hammersley, ESRF, Grenoble,  
11 France). Fiber anisotropy plots were then produced for each image by phase-shifting the  
12 aligned fiber component of the azimuthal intensity profile (clear region in Fig. 3C) by  
13 90° and displaying the resulting graphs in polar coordinates (Fig. 3D), analogous to the  
14 polar vector representation used for the WAXS data. An accompanying anisotropy  
15 value was calculated for each plot by computing the ratio of the integrals of the aligned  
16 and aligned-plus-isotropic components of the azimuthal intensity distribution (Fig. 3C),  
17 following the convention used in the WAXS analysis. Each anisotropy value was then  
18 normalised against the maximal value in the sequence to give a measure of the relative  
19 degree of circumferential alignment with respect to tissue depth.

20

## 21 **RESULTS**

22

### 23 **X-ray Scattering**

1            Fig. 4 shows polar vector maps of preferential collagen fiber orientation in left  
2 and right posterior scleras of a non-glaucoma donor (n1). Supplementary Fig. S1 shows  
3 equivalent data from the left eye of a second non-glaucoma donor (n2). The maps  
4 indicate that fiber orientation in the mid-posterior sclera was anisotropic and  
5 inhomogeneous. Although fiber arrangement was evidently complex, the predominantly  
6 two-fold and four-fold symmetry of the individual plots indicates that, at any given  
7 position, fiber anisotropy could be represented in terms either one (from here onwards  
8 referred to as 'uniaxial') or two ('biaxial') preferential fiber directions with associated  
9 dispersions. The peripapillary sclera was characterized by a circumferential alignment  
10 of fibers parallel to the scleral canal. In addition, notable meridional fiber bands radiated  
11 tangentially from the superior and inferior regions of the peripapillary collagen ring in  
12 superior-nasal and inferior-nasal directions respectively, rendering a degree of mirror  
13 symmetry between left and right eyes (Fig. 4C,D - arrows). Although there was some  
14 variation in the bulk direction of fibers in the mid-posterior sclera between individual  
15 specimens, these dominant structural features were highly reproducible, and were also  
16 found in all 4 of the remaining non-glaucoma scleras examined (data not shown).

17 Equivalent polar vector maps from a pair of scleras from a glaucoma donor (g1), and a  
18 left sclera from second glaucoma donor (g2), are shown in Figs. 5 and S2 respectively.  
19 The structural features identified in the non-glaucoma specimens were also evident in  
20 all 5 of the glaucoma eyes examined (of which 3 are shown here). Similar to non-  
21 glaucoma specimens, some individual variation in bulk fiber direction was evident in  
22 the mid-posterior sclera. However, no notable overall differences were found between  
23 non-glaucoma and glaucoma specimens in terms of bulk fiber direction.

1           The color coding of the individual polar vector plots in Figs. 4 ,5, S1 and S2  
2 suggested that the degree of fiber anisotropy varied with position across each specimen.  
3 In general, the peripapillary fiber ring appeared considerably more highly aligned than  
4 the mid-posterior collagen. In order to further quantify this, we computed the  
5 anisotropic ratio of aligned to total collagen scatter (Fig. 1C). These values are  
6 displayed as contour maps in Fig. 6. For both non-glaucoma and glaucoma specimens,  
7 the degree of anisotropy was confirmed to be, on average, 37% higher in the  
8 peripapillary region compared to the mid-posterior. Moreover the degree of anisotropy  
9 in the peripapillary ring varied markedly (between 2-fold and 4-fold) with  
10 circumferential position around the scleral canal. The distribution pattern of scleral fiber  
11 anisotropy varied between specimens within both groups, and this variation was  
12 particularly evident in the peripapillary region (Fig. 6), however minimum peripapillary  
13 anisotropy was observed in the superior-nasal quadrant in 6/7 of non-glaucoma and 4/5  
14 of glaucoma scleras (Fig. 6). Regional and average fiber anisotropy did not differ  
15 significantly between non-glaucoma and glaucoma groups in the mid-posterior sclera  
16 (Table 2). In contrast, fiber anisotropy was significantly reduced in the superior-  
17 temporal ( $p < 0.01$ ) and inferior-nasal ( $p < 0.05$ ) quadrants of the peripapillary tissue in  
18 glaucoma eyes compared to non-glaucoma (Table 2). **Regional measures of fiber**  
19 **anisotropy were not statistically different between the 4 diabetic eyes and the 8 non-**  
20 **diabetic eyes studied ( $p > 0.05$ ).**

21

## 22 **Multiphoton Microscopy**

23           Second harmonic generation signals from fibrous collagen were clearly visible  
24 in the peripapillary scleral sections examined using multiphoton imaging (Fig. 7A-F, S).

1 In the inner (i.e. proximal to the choroid) one-third of the peripapillary sclera from non-  
2 glaucoma specimen n4r, highly interwoven fibril bundles were observed crossing at  
3 random angles (Fig. 7A, B). Thereafter, when traversing the tissue thickness in an  
4 outward direction, collagen bundles appeared progressively less-interwoven and more  
5 highly aligned circumferential to the scleral canal (Fig. 7C-E), before becoming less  
6 aligned again in the most superficial one-sixth of the sclera (Fig. 7F). FFT analysis of  
7 multiphoton images confirmed fiber anisotropy was higher in the mid-to-outer stroma  
8 compared to the inner sclera (Fig. 7(G-L, M-R), with peak anisotropy always occurring  
9 in the depth range: 200-500 $\mu$ m (Fig. 7T). A similar trend was observed in the  
10 peripapillary sclera of glaucoma specimen g3r (Fig. 8). These features were confirmed  
11 in a further specimen from each group, n6r and g11 (see Supplementary Fig. S3). Mean  
12 and standard deviations for the depth at which peak fiber anisotropy was observed, per  
13 eye, were: n4r (388 $\mu$ m  $\pm$  144), n6r (350 $\mu$ m  $\pm$  123), g3r (275 $\mu$ m  $\pm$  87), g11 (300 $\mu$ m  $\pm$   
14 87). Further experimental work, using a larger multiphoton specimen size, is required  
15 to determine whether the depth-dependency of the fiber orientation varies significantly  
16 between non-glaucoma and glaucoma eyes.

17

18

## 19 **DISCUSSION**

20 The WAXS results presented here indicate that the human posterior sclera is  
21 highly anisotropic, and that both the direction and degree of anisotropy vary markedly  
22 across the tissue. This fits well with mechanical<sup>26, 27</sup> and histological findings<sup>16</sup> in  
23 human eyes. Our reporting of biaxial preferential fiber alignment in regions of the mid-  
24 posterior sclera (Figs 4, 5, S1 and S2) is likely due to bands of collagen at various

1 depths in the tissue crossing at large angles, as implied by Kokott's early work<sup>16</sup>. With  
2 this in mind, it should be remembered that our WAXS method yields thickness-  
3 averaged data, and cannot reveal depth-dependent information. Moreover, multiple  
4 collagen bands crossing at more acute angles may be assimilated by WAXS into a  
5 common distribution about a single dominant preferred direction. In these respects,  
6 WAXS presents a highly quantitative yet simplified view of the full tissue architecture.

7         Our observation of a highly reinforced circumferential ring of collagen fibers in  
8 the peripapillary sclera (Figs. 4, 5, S1 and S2) is consistent with previous qualitative  
9 imaging of human tissue<sup>16, 20, 28</sup>. Such an arrangement is also predicted by measurements  
10 of IOP-driven scleral deformation in monkeys<sup>29</sup> and humans<sup>12</sup>. It is possible that this  
11 ring forms some protective function for the optic nerve axons, since numerical  
12 modelling has shown that a circular arrangement of fibers around the scleral canal is  
13 biomechanically optimal in order to minimize lamina expansion as IOP is altered<sup>30</sup>. The  
14 oblique meridional fibers associated with the superior and inferior peripapillary sclera  
15 (Figs. 4, 5, S1 and S2) are also consistent with early histological observations<sup>16</sup>, and  
16 may conceivably have some additional stabilising role in relation to the optic nerve  
17 head.

18         A further interesting result of the current study was that the degree of fiber  
19 anisotropy within the peripapillary ring varied markedly (up to four-fold) with  
20 circumferential position around the scleral canal (Fig. 6), and that weakest  
21 circumferential alignment was consistently observed in the superior-nasal quadrant (Fig.  
22 6 and Table 2). Moreover, the multiphoton imaging we carried out revealed that this  
23 structure does not extend through the full thickness of the tissue, but instead is formed  
24 mainly by fibers lying in the mid-to-outer stroma and encompassing only about 50% of

1 the total scleral thickness (Figs. 7 and 8). We suggest that there would be some value in  
2 considering these features in future numerical simulations aimed at predicting IOP-  
3 derived lamina strain.

4         There is evidence that connective tissue remodelling in glaucoma extends  
5 beyond the lamina into the peripapillary sclera<sup>11, 13-15</sup>. Notably, studies of glaucomatous  
6 human eyes using electron microscopy have indicated a decrease in peripapillary  
7 collagen fibril density<sup>15</sup> and an uncoupling of the elastin and collagen matrix  
8 components<sup>14</sup>. Whether this apparent remodelling extends to the level of collagen fiber  
9 alignment has not been addressed experimentally. The current study indicated that the  
10 general pattern of bulk fiber directions in posterior human sclera was similar between  
11 non-glaucoma donors and those with a history of glaucoma and confirmed axon loss  
12 (Figs. 4, 5, S1 and S2). In the context of our observation, it is interesting to note that a  
13 recent modelling study using monkey sclera has also suggested no change in bulk fiber  
14 direction between non-glaucoma and glaucoma eyes<sup>31</sup>. However, the present study did  
15 indicate significant regional differences in mean fiber *anisotropy* within the  
16 peripapillary sclera between non-glaucoma and glaucoma eyes, while, in contrast, no  
17 such differences were found in the mid-posterior tissue (Table 2). It is possible that  
18 these differences represent some adaptive change in response to glaucoma, or else might  
19 be baseline structural properties that associate with predisposition to glaucomatous axon  
20 damage. The course of scleral fibers within a given eye cannot be compared before and  
21 after glaucoma onset in a human post-mortem study such as ours, and therefore the  
22 current results can neither confirm nor distinguish between these two possible  
23 interpretations. Further studies characterising the time-course of fiber anisotropy during  
24 disease development in experimental glaucoma are encouraged.

1           The regional differences in peripapillary fiber anisotropy between normal and  
2 damaged glaucoma eyes identified herein may be relevant biomechanically. Of interest,  
3 a recent study reported differing meridional strain behavior in the peripapillary region of  
4 age-matched control and damaged glaucoma human scleras subjected to inflation tests,  
5 while mid-posterior stress-strain behaviour was similar between the groups<sup>12</sup>. With this  
6 in mind, it is relevant to note that the mechanical stiffness of the sclera, or its resistance  
7 to deformation, is influenced by both geometric and material parameters<sup>5, 6, 31</sup>. Further  
8 research is required to determine exactly how the interplay between scleral size, shape,  
9 thickness and fiber arrangement within a given eye governs its individual response to  
10 IOP change, particularly given the inter-specimen variations in fiber anisotropy  
11 indicated by the current WAXS data.

12           As mentioned above, it is important to note that the WAXS method we have  
13 used here is inherently limited in its inability to determine the depth dependency of the  
14 preferred orientation of scleral collagen. Quantitative depth-profiling of sclera is  
15 potentially achievable by combining WAXS with serial tissue sectioning, as  
16 demonstrated by corneal studies<sup>32, 33</sup>. In addition, our study was subject to a number of  
17 further experimental limitations. Firstly, there was the effect of the scleral curvature.  
18 With increasing distance from the nerve head, the effective tissue thickness presented to  
19 the x-ray beam is increasingly elevated by the curvature, with a proportional increase in  
20 total (i.e. isotropic and aligned) x-ray scatter, affecting the relative size of the polar  
21 vector plots in Figs. 4, 5, S1 and S2. The estimated increase in scatter due to scleral  
22 curvature was calculated to be <2% in the peripapillary region, increasing to ~17% at  
23 the specimen periphery (based a posterior scleral radius of curvature of 12mm).  
24 However, it is important to note that curvature would not have affected the relative fiber

1 number as a function of angle *within a given polar vector plot* (indicated by the *shape*  
2 of the individual plots). Neither would it have affected the fiber anisotropy  
3 measurements (Fig. 6), which are thickness-independent<sup>22</sup>. To characterise fiber  
4 orientation across the whole posterior sclera without dissection will require a tilting  
5 specimen cell to maintain the incident x-ray beam perpendicular to the tissue surface.  
6 This is currently under development.

7         The second limitation concerns the hierarchical structure of collagen. Since  
8 WAXS is a molecular signal<sup>22</sup>, the helicoidal packing of the microfibrillar subunits  
9 comprising the fibers will contribute to the angular smearing of the WAXS diffraction  
10 peaks shown in Fig. 1A, leading to an under-estimation in the degree of fiber anisotropy  
11 measured by WAXS. In sclera the microfibrillar tilt angle with respect to the fiber axis  
12 is relatively small ( $\sim 5^\circ$ )<sup>18</sup>, and therefore we anticipate our under-estimation of  
13 anisotropy by WAXS to be accordingly minor. The multiphoton signal derives from  
14 fibril bundles, and is therefore not subject to this error. However, the difference in  
15 signal origin should be born in mind when comparing data from the WAXS and  
16 multiphoton methods. The size of collagen fibril bundle structures detected by  
17 multiphoton imaging is highly variable, predicting a radially diffuse FFT pattern (see  
18 Figs. 7 and 8), whereas WAXS has the advantage that the collagen molecular diameter  
19 is, in contrast, highly uniform, leading to a much sharper, more well-resolved signal  
20 (see Fig. 1). Moreover, a proportion of the fibrillar structures in the multiphoton images  
21 are obscured to the FFT processing by the interwoven nature of the sclera (Figs. 7 and  
22 8), whereas WAXS is not affected. Owing to these limitations, in the current paper  
23 quantification of fiber anisotropy from multiphoton data is limited to reporting of  
24 *relative, normalised* values only. Any study which makes a comparison between

1 *absolute* values of fiber anisotropy as measured using imaging and scattering methods  
2 should consider the above-mentioned factors.

3         Thirdly, it is likely that some, if not all, of the human scleras used in this study  
4 were from donors affected with varying degrees of refractive error. It is unknown  
5 whether bulk scleral fiber orientation is affected in myopia. However, there is extensive  
6 evidence from both human and animal myopia studies that the posterior scleral matrix  
7 remodels at the level of the collagen fibrils during myopic eye growth<sup>34, 35</sup>. While  
8 refractive information was not available for the scleras used in our study, measurements  
9 of ocular dimensions post-mortem did not indicate any significant differential trend  
10 between the non-glaucoma and glaucoma groups (Table 1). Nevertheless, it is possible  
11 that inter-specimen differences in myopic status may have made some contribution to  
12 the large differences in anisotropy between eyes indicated herein.

13         Lastly, there are inherent difficulties in confirming glaucoma status in human  
14 eyes obtained post-mortem from eye bank sources. Many previous studies have  
15 accepted the statement from the providing agency that the patient had glaucoma, owing  
16 to increasing difficulties in obtaining detailed medical records of glaucoma diagnosis  
17 and treatment due of Federal privacy regulations. In a recent publication<sup>12</sup>, we evaluated  
18 optic nerve cross-sections of glaucoma eyes using a previously validated histological  
19 method<sup>24</sup>, and were able to assess the severity of axonal damage in 20 out of 24  
20 specimens. The ungradable nerves had suffered post-mortem autolysis. We have used  
21 the same methodology here to verify glaucoma status in eyes obtained from NDRI.  
22 Other investigators are encouraged to perform optic nerve damage assessment by some  
23 histological method to validate glaucoma status in the eye bank tissues that they use.

1           In summary, we have used WAXS and multiphoton imaging to quantitatively  
2 map the orientation of collagen in the peripapillary and mid-posterior human sclera,  
3 showing that the bulk fiber arrangement at any given point in the tissue can be  
4 simplified into uniaxial or biaxial distributions. As such, the data is highly amenable for  
5 inclusion in inverse finite-element simulation. Given the considerable variation in  
6 anisotropy between specimens highlighted by the current study, we suggest that  
7 experimental fiber orientation data should be assimilated into human eye models, along  
8 with associated morphometric and thickness parameters, on an individual-specific basis.  
9 This work is currently on-going in our lab. Quantitative structural information on  
10 human sclera of the kind presented here will help to improve our understanding of the  
11 tissue's mechanical influence on the optic nerve head, and thereby the sclera's possible  
12 role in glaucoma.

13

#### 14 *Acknowledgements*

15

16 The authors thank Dr Nick White of Vision Sciences Bioimaging Laboratories, Cardiff  
17 University, for advice concerning the non-linear microscopy. This work was funded by  
18 Fight for Sight Grant 1360 (to CB and KMM), NIH Grants EY021500 (to TDN) and  
19 EY02120, EY01765 (to HAQ), and USAMRMC Award W81XWH-10-1-0766 (to  
20 TDN). The Diamond Light Source is supported by the Science and Technologies  
21 Facilities Council.

22

#### 23 *References*

24 **1. Watson PG, Young RD. Scleral structure, organisation and disease. A**  
25 **review. *Experimental Eye Research* 2003;78:609-623.**

- 1 2. Girard MJ, Downs JC, Bottlang M, Burgoyne CF, Suh JK. Peripapillary  
2 and Posterior Scleral Mechanics-Part II: Experimental and Inverse Finite Element  
3 Characterization. *J Biomech Eng* 2009;131:051012.
- 4 3. Burgoyne CF, Downs JC. Premise and prediction-how optic nerve head  
5 biomechanics underlies the susceptibility and clinical behavior of the aged optic  
6 nerve head. *J Glaucoma* 2008;17:318-328.
- 7 4. Downs JC, Roberts MD, Burgoyne CF. Mechanical environment of the  
8 optic nerve head in glaucoma. *Optom Vis Sci* 2008;85:425-435.
- 9 5. Eilaghi A, Flanagan JG, Simmons CA, Ethier CR. Effects of scleral stiffness  
10 properties on optic nerve head biomechanics. *Ann Biomed Eng* 2010;38:1586-1592.
- 11 6. Norman RE, Flanagan JG, Sigal IA, Rausch SM, Tertinegg I, Ethier CR.  
12 Finite element modeling of the human sclera: Influence on optic nerve head  
13 biomechanics and connections with glaucoma. *Exp Eye Res* 2010;Sept 29.
- 14 7. Sigal IA, Flanagan JG, Tertinegg I, Ethier CR. Modeling individual-specific  
15 human optic nerve head biomechanics. Part II: influence of material properties.  
16 *Biomech Model Mechanobiol* 2009;8:99-109.
- 17 8. Sigal IA, Ethier CR. Biomechanics of the optic nerve head. *Exp Eye Res*  
18 2009;88:799-807.
- 19 9. Quigley HA, Addicks EM, Green WR, Maumenee AE. Optic nerve damage  
20 in human glaucoma. II. The site of injury and susceptibility to damage. *Arch*  
21 *Ophthalmol* 1981;99:635-649.
- 22 10. Sigal IA. Interactions between geometry and mechanical properties on the  
23 optic nerve head. *Invest Ophthalmol Vis Sci* 2009;50:2785-2795.
- 24 11. Norman RE, Flanagan JG, Rausch SM, et al. Dimensions of the human  
25 sclera: Thickness measurement and regional changes with axial length. *Exp Eye*  
26 *Res* 2010;90:277-284.
- 27 12. Coudrillier B, Tian J, Alexander S, Myers KM, Quigley HA, Nguyen TD.  
28 Mechanical response of the human posterior sclera: age and glaucoma related  
29 changes measured using inflation testing. *Invest Ophthalmol Vis Sci* 2012;53:1714-  
30 1728.
- 31 13. Downs JC, Suh JK, Thomas KA, Bellezza AJ, Hart RT, Burgoyne CF.  
32 Viscoelastic material properties of the peripapillary sclera in normal and early-  
33 glaucoma monkey eyes. *Invest Ophthalmol Vis Sci* 2005;46:540-546.
- 34 14. Quigley HA, Brown A, Dorman-Pease ME. Alterations in elastin of the  
35 optic nerve head in human and experimental glaucoma. *Br J Ophthalmol*  
36 1991;75:552-557.
- 37 15. Quigley HA, Dorman-Pease ME, Brown AE. Quantitative study of collagen  
38 and elastin of the optic nerve head and sclera in human and experimental monkey  
39 glaucoma. *Curr Eye Res* 1991;10:877-888.
- 40 16. Kokott W. Das spaltlinienbild der sklera (Ein beitrag zum funktionellen  
41 bau der sklera) *Klin Monbl Augenheilkd* 1934;92:177-185.
- 42 17. Marshall GE, Konstas AGP, Lee WR. Collagens in ocular tissues. *British*  
43 *Journal of Ophthalmology* 1993;77:515-524.
- 44 18. Yamamoto S, Hashizume H, Hitomi J, et al. The subfibrillar arrangement  
45 of corneal and scleral collagen fibrils as revealed by scanning electron and atomic  
46 force microscopy. *Archives of Histology and Cytology* 2000;63:127-135.

- 1 19. Yan D, McPheeters S, Johnson G, Utzinger U, Vande Geest J.  
2 Microstructural Differences in the Human Posterior Sclera As a Function of Age  
3 and Ethnicity. *Invest Ophthalmol Vis Sci* 2010;Nov 4. .
- 4 20. Winkler M, Jester B, Nien-Shy C, et al. High resolution three-dimensional  
5 reconstruction of the collagenous matrix of the human optic nerve head. *Brain*  
6 *Research Bulletin* 2010;81:339-348.
- 7 21. Girard MJ, Dahlmann-Noor A, Rayapureddi S, et al. Quantitative mapping  
8 of scleral fiber orientation in normal rat eyes. *Invest Ophthalmol Vis Sci*  
9 2011;52:9684-9693.
- 10 22. Meek KM, Boote C. The use of x-ray scattering techniques to quantify the  
11 orientation and distribution of collagen in the corneal stroma. *Prog Retin Eye Res*  
12 2009;28:369-392.
- 13 23. Boote C, Hayes S, Abahussin M, Meek KM. Mapping collagen organisation  
14 in the human cornea: left and right eyes are structurally distinct. *Invest*  
15 *Ophthalmol Vis Sci* 2006;47:901-908.
- 16 24. Kendell KR, Quigley HA, Kerrigan LA, Pease ME, Quigley EN. Primary  
17 Open-Angle Glaucoma is not Associated with Photoreceptor Loss. *Investigative*  
18 *Ophthalmology & Visual Science* 1995;36:200-205.
- 19 25. Boote C, Elsheikh A, Kassem W, et al. The Influence of Lamellar  
20 Orientation on Corneal Material Behavior: Biomechanical and Structural  
21 Changes in an Avian Corneal Disorder. *Investigative Ophthalmology & Visual*  
22 *Science* 2011;52:1243-1251.
- 23 26. Bisplinghoff JA, McNally C, Manoogian SJ, Duma SM. Dynamic material  
24 properties of the human sclera. *J Biomech* 2009;42:1493-1497.
- 25 27. Elsheikh A, Geraghty B, Alhasso D, Knappett J, Campanelli M, Rama P.  
26 Regional variation in the biomechanical properties of the human sclera. *Exp Eye*  
27 *Res* 2010;90:624-633.
- 28 28. Morrison JC, Lhernault NL, Jerdan JA, Quigley HA. Ultrastructural  
29 Location of Extracellular-Matrix Components in the Optic Nerve Head. *Archives*  
30 *of Ophthalmology* 1989;107:123-129.
- 31 29. Girard MJ, Suh JK, Bottlang M, Burgoyne CF, Downs JC. Scleral  
32 Biomechanics in the Aging Monkey Eye. *Invest Ophthalmol Vis Sci* 2009;50:5226-  
33 5237.
- 34 30. Grytz R, Meschke G, Jonas JB. The collagen fibril architecture in the  
35 lamina cribrosa and peripapillary sclera predicted by a computational remodeling  
36 approach. *Biomech Model Mechanobiol* 2011;10:371-382.
- 37 31. Girard MJ, Suh JK, Bottlang M, Burgoyne CF, Downs JC. Biomechanical  
38 Changes in the Sclera of Monkey Eyes Exposed to Chronic IOP Elevations. *Invest*  
39 *Ophthalmol Vis Sci* 2011.
- 40 32. Abahussin M, Hayes S, Knox Cartwright NE, et al. 3D collagen orientation  
41 study of the human cornea using X-ray diffraction and femtosecond laser  
42 technology. *Invest Ophthalmol Vis Sci* 2009;50:5159-5164.
- 43 33. Kamma-Lorger CS, Boote C, Hayes S, et al. Collagen and mature elastic  
44 fibre organisation as a function of depth in the human cornea and limbus. *J Struct*  
45 *Biol* 2010;169:424-430.
- 46 34. McBrien NA, Jobling AI, Gentle A. Biomechanics of the sclera in myopia:  
47 extracellular and cellular factors. *Optom Vis Sci* 2009;86:E23-30.

1 **35. Rada JAS, Shelton S, Norton TT. The sclera and myopia. *Experimental Eye***  
2 ***Research* 2006;82:185-200.**

3

4

5 **FIGURE LEGENDS**

6

7 **Figure 1:** (A) WAXS pattern from the peripapillary region of human sclera. The two-  
8 lobed appearance of the collagen intermolecular x-ray reflection is indicative of uniaxial  
9 fiber alignment in the direction of the arrow. *Inset:* Example of a four-lobed WAXS  
10 pattern from the mid-posterior sclera, indicative of biaxial fiber alignment. (B) Power-  
11 law background function (broken line) fitted to a radial profile (solid line) through  
12 pattern shown in (A). For each pattern, 256 individual such background functions were  
13 fitted and subtracted along 256 equally spaced radial directions, enabling the collagen  
14 signal to be isolated and extracted in two dimensions. *Arrow:* Collagen signal peak. (C)  
15 Angular x-ray scatter intensity profile of pattern shown in (A). The scatter may be  
16 separated into that arising from isotropically arranged collagen fibers (shaded region)  
17 and that arising from preferentially oriented fibers (clear region). (D) Aligned collagen  
18 scatter displayed as a polar vector plot, whose shape reveals the collagen anisotropy.  
19 The length of any line drawn from the centre of the plot to its edge in a given direction  
20 is proportional to the relative number of fibers preferentially aligned in that direction.  
21 (E) Multiphoton microscopy image from mid-stromal depth, taken from the same  
22 specimen and region as the WAXS data. Second harmonic signals reveal highly aligned  
23 collagen fibril bundles, in agreement with the fiber orientation measurement by WAXS.

24

1 **Figure 2:** (A) A fixed-size region (shaded), encompassing 64 measurement points,  
2 representing the peripapillary sclera (ppScl) was identified for each specimen. All data  
3 points outside this region were considered mid-posterior sclera (mpScl). (B) ppScl  
4 region overlaid on fiber polar vector map for specimen n4r. The ppScl region was  
5 identified based on the x-ray scatter drop-out in the nerve head and the presence of  
6 strong circumferential fiber alignment indicated by the polar vectors. The scaling of the  
7 vectors is related to the degree of anisotropy. To allow montage display, the larger plots  
8 (indicative of higher fiber anisotropy) have been scaled down by the factors indicated in  
9 the color key. (C) ppScl region (solid line) overlaid on contour map of calculated fiber  
10 anisotropy. The mpScl and ppScl regions were sub-divided into their 4 principal  
11 quadrants (shown demarcated by broken lines), and the mean anisotropy values within  
12 each region were statistically compared between non-glaucoma and glaucoma groups.

13

14 **Figure 3:** (A) Multiphoton microscopy image of collagen fibril bundles in the outer  
15 stroma of the peripapillary sclera. (B) Fast Fourier transform (FFT, theoretical  
16 diffraction pattern) from image in (A). The degree of eccentricity in the pattern relates  
17 to degree of fiber alignment. (C) Angular intensity profile of FFT shown in (B). The  
18 distribution may be separated into that arising from isotropically arranged collagen  
19 fibers (shaded region) and that arising from preferentially oriented fibers (clear region).  
20 (D) Aligned collagen signal displayed as a polar vector plot, whose shape reveals the  
21 collagen anisotropy. The length of any line drawn from the centre of the plot to its edge  
22 in a given direction is related to the relative number of fibers preferentially aligned in  
23 that direction.

24

1 **Figure 4: (A,B)** Polar vector maps of preferential collagen fiber orientation across  
2 15mm diameter posterior scleral specimens (n1l and n1r) from a pair of non-glaucoma  
3 human eyes, sampled at 0.5mm intervals, and viewed from the posterior side. The  
4 scaling of the vectors is related to the degree of anisotropy. To allow montage display,  
5 the larger plots (indicative of higher fiber anisotropy) have been scaled down by the  
6 factors indicated in the color key. Superior (S), inferior (I), nasal (N) and temporal (T)  
7 specimen positions are marked. The left eye has been mirror-flipped horizontally to  
8 enable direct comparison with the right eye. (C,D) Polar vector plots mapped onto 3D  
9 posterior eye models. Dominant features of the fiber structure are indicated by arrows:  
10 note circumferential fibers ringing the optic nerve head (ONH) and the oblique splaying  
11 of meridional fibers from the ring toward the S-N and I-N directions. (E,F) Regional  
12 maps showing average polar plots within the 4 principal quadrants of the peripapillary  
13 sclera and 16 regions of the mid-posterior tissue.

14

15 **Figure 5: (A,B)** Polar vector maps of preferential collagen fiber orientation across  
16 15mm diameter posterior scleral specimens (g1l and g1r) from a pair of glaucoma  
17 human eyes, sampled at 0.5mm intervals, and viewed from the posterior side. The left  
18 eye has been mirror-flipped horizontally to enable direct comparison with the right eye.  
19 (C,D) Polar vector plots mapped onto 3D posterior eye models. Note the overall  
20 arrangement of fibers is similar to non-glaucoma eyes. (E,F) Regional maps showing  
21 average polar plots within the 4 principal quadrants of the peripapillary sclera and 16  
22 regions of the mid-posterior tissue.

23

1 **Figure 6:** *Left panel:* Contour maps of fiber anisotropy for non-glaucoma human  
2 posterior scleras, viewed from the posterior side. The left eyes have been mirror-flipped  
3 horizontally to enable direct comparison with the right eyes. Colour key shows degree  
4 of anisotropy expressed as proportion of aligned to total collagen fiber x-ray scatter.  
5 Grid element: 0.5mm. Mean regional anisotropy within the principal quadrants of the  
6 peripapillary and mid-posterior regions are shown alongside each map. The superior  
7 (S), inferior (I), nasal (N) and temporal (T) poles are indicated. *Right panel:* Equivalent  
8 data for glaucoma specimens. Note the large variation in peripapillary anisotropy with  
9 position around the scleral canal for both groups. Mid-posterior regional averages are  
10 not shown for specimen n4r, due to this being a partial WAXS scan.

11

12 **Figure 7:** (A-F) Multiphoton images from peripapillary sclera of non-glaucoma human  
13 eye n4r - second harmonic generation signals reveal collagen fibril bundle arrangement.  
14 The left to right image sequence shows a depth profile at a single location (region 1 in  
15 panel S), traversing the scleral thickness in an inner (choroid side) to outer direction at  
16 the depths indicated. Note that mid/outer stromal collagen fibril bundles are less  
17 interwoven and more highly aligned in (C-E), before becoming less aligned in the  
18 outermost layer in (F). (G-L) Fast Fourier transforms (FFT, theoretical diffraction  
19 patterns) calculated from the images in (A-F). The eccentricity of the patterns is related  
20 to the degree of fiber anisotropy. (M-R) Polar vector plots of preferential fiber  
21 orientation, calculated from FFTs. The same scaling was used for all plots. Relative  
22 anisotropy (normalised to the maximum value in the sequence) is shown alongside each  
23 plot. (S) Reconstruction of  $15 \times 15$  multiphoton image tiling of whole peripapillary  
24 sclera at a depth of  $500\mu\text{m}$ , showing fibrillar collagen circumferential to the optic nerve

1 head (ONH). The white rectangles denotes the four locations at the which depth-profiles  
2 were recorded. (T) Graph showing normalised fiber anisotropy as a function of tissue  
3 depth at the four locations shown in panel S.

4

5 **Figure 8:** (A-F) Multiphoton image depth profile from peripapillary sclera of glaucoma  
6 human eye g3r, recorded from region 1 (see panel S for location). (G-L) Fast Fourier  
7 transforms (theoretical diffraction patterns) of images shown in (A-F). (M-R) Polar  
8 vector plots and normalised anisotropy values calculated from FFTs. The same scaling  
9 was used for all plots. (S) Reconstruction of whole peripapillary sclera at a depth of  
10 500 $\mu\text{m}$ . The white rectangles denotes the four locations at the which depth-profiles were  
11 recorded. (T) Graph showing normalised fiber anisotropy as a function of tissue depth  
12 at the four locations shown in panel S. Note that the depth-dependency of the fiber  
13 anisotropy follows that of the non-glaucoma specimen.

14

15

16

17

18

19

20

21

22

23

24

1 **TABLES**

2

3 **TABLE 1:** Details of the Caucasian human scleras used in the study. Dimensions refer  
 4 to superior-inferior (SI) and nasal-temporal (NT) globe diameters and axial length (AL)  
 5 in mm. \* left/right pair from the same donor. † data not recorded.

Sclera	Left/ Right	Age	Sex	Non-glaucoma/ Glaucoma	Nerve Grade	Diabetes	Dimensions		
							SI	NT	AL
n1l*	L	77	F	N	0	No	24.4	24.2	23.9
n1r*	R	77	F	N	0	No	24.4	24.6	23.9
n2l	L	74	F	N	0	Type II	24.8	25.1	25.3
n3r	R	77	M	N	0	No	24.2	24.7	24.8
n4r	R	71	F	N	0	No	23.1	22.1	23.5
n5r	R	91	F	N	0	No	22.4	23.0	22.7
n6r	R	67	F	N	0	Type I	22.6	23.0	23.1
g1l*	L	81	F	G	3	No	24.1	23.7	23.4
g1r*	R	81	F	G	3	No	23.4	23.9	24.4
g2l	L	82	M	G	3	Type II	25.1	25.9	25.2
g3r	R	63	M	G	2	Type II	†	†	†
g4r	R	63	M	G	2	No	24.2	24.5	24.3

6

7

8

9

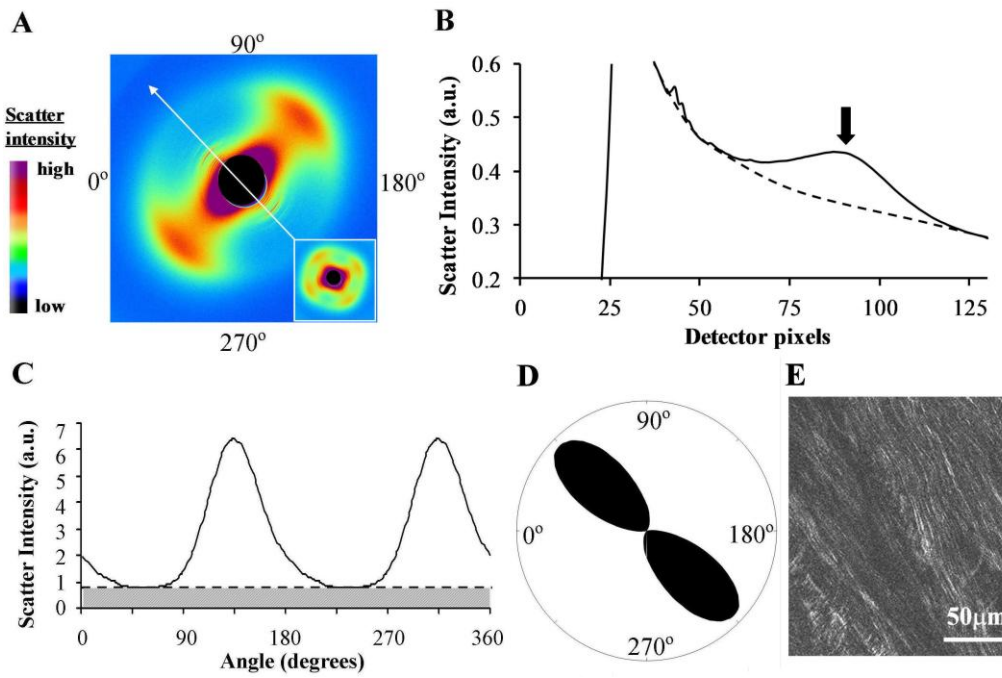
10

1 **TABLE 2:** Comparison of collagen fiber anisotropy by scleral region between non-  
 2 glaucoma and glaucoma groups, as measured using WAXS. Notation - MP: mid-  
 3 posterior sclera, PP: peripapillary sclera, SN: superior-nasal quadrant, ST: superior-  
 4 temporal quadrant, IN: inferior-nasal quadrant, IT: inferior-temporal quadrant.  
 5 Statistical significance is indicated at the \* $p < 0.05$  and \*\* $p < 0.01$  levels.  
 6

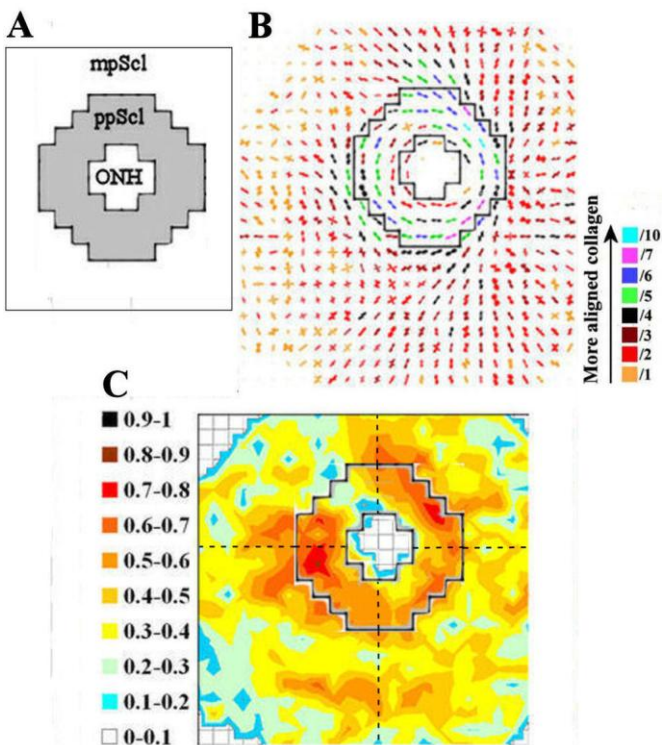
Region	Non-glaucoma		Glaucoma	
	<u>Mean</u>	<u>(var.)</u>	<u>Mean</u>	<u>(var.)</u>
MP-SN	0.32	(0.02)	0.35	(0.02)
MP-ST	0.36	(0.02)	0.35	(0.02)
MP-IN	0.34	(0.01)	0.32	(0.02)
MP-IT	0.33	(0.02)	0.31	(0.05)
MP-all	0.34	(0.02)	0.33	(0.02)
PP-SN	0.39	(0.03)	0.37	(0.02)
PP-ST	0.55	(0.01)**	0.47	(0.03)**
PP-IN	0.49	(0.01)*	0.45	(0.01)*
PP-IT	0.46	(0.01)	0.50	(0.02)
PP-all	0.47	(0.02)	0.45	(0.02)

7

8

1 **FIGURES**

2

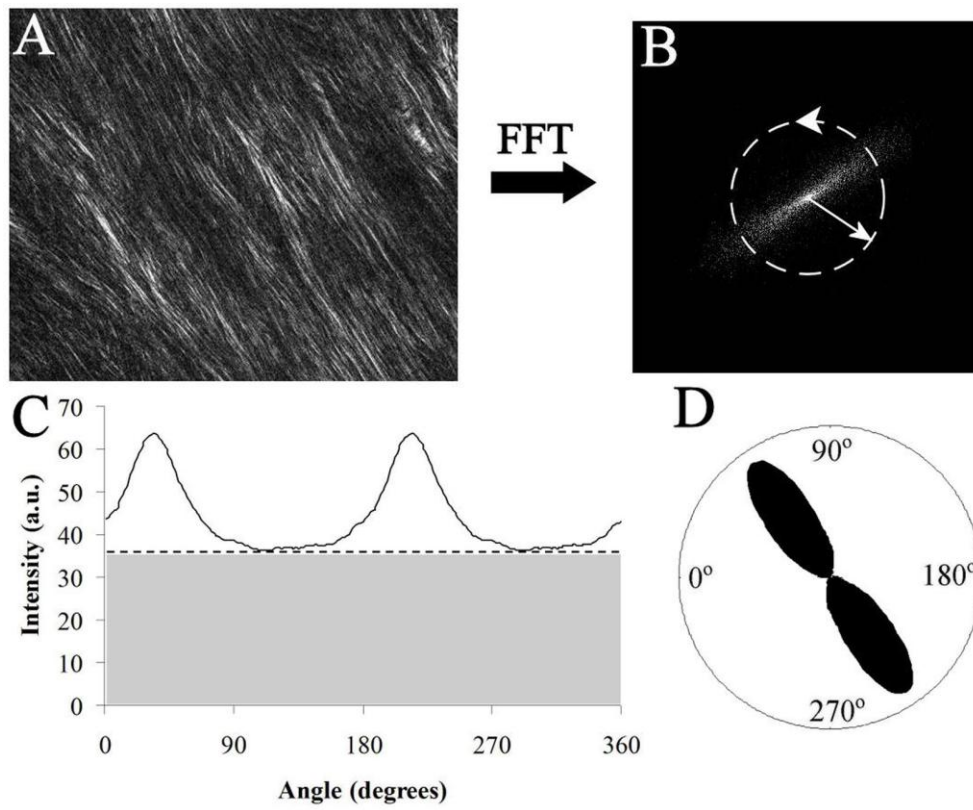
3 **Figure 1**

4

5 **Figure 2**

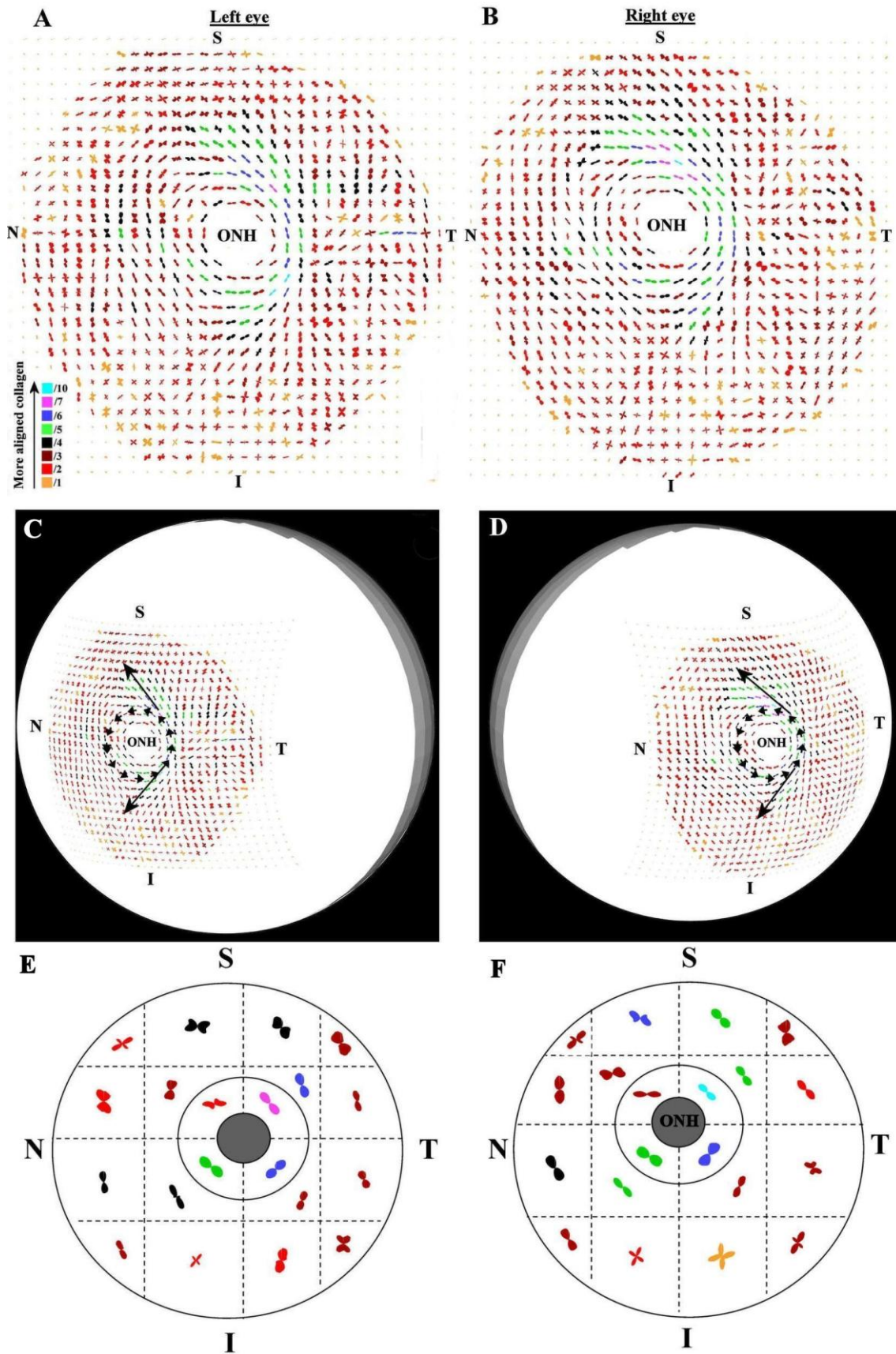
6

1



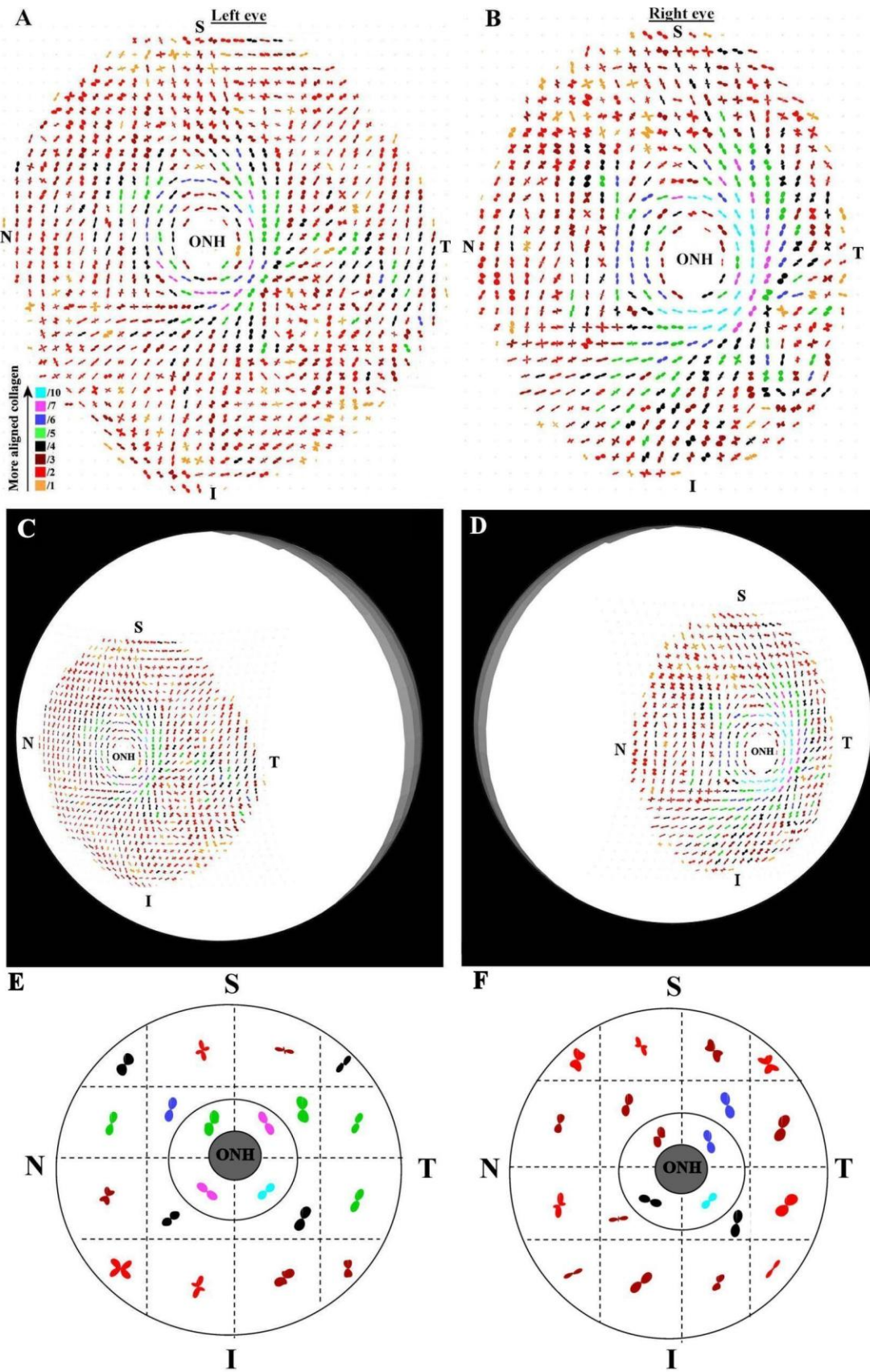
2

3 **Figure 3**



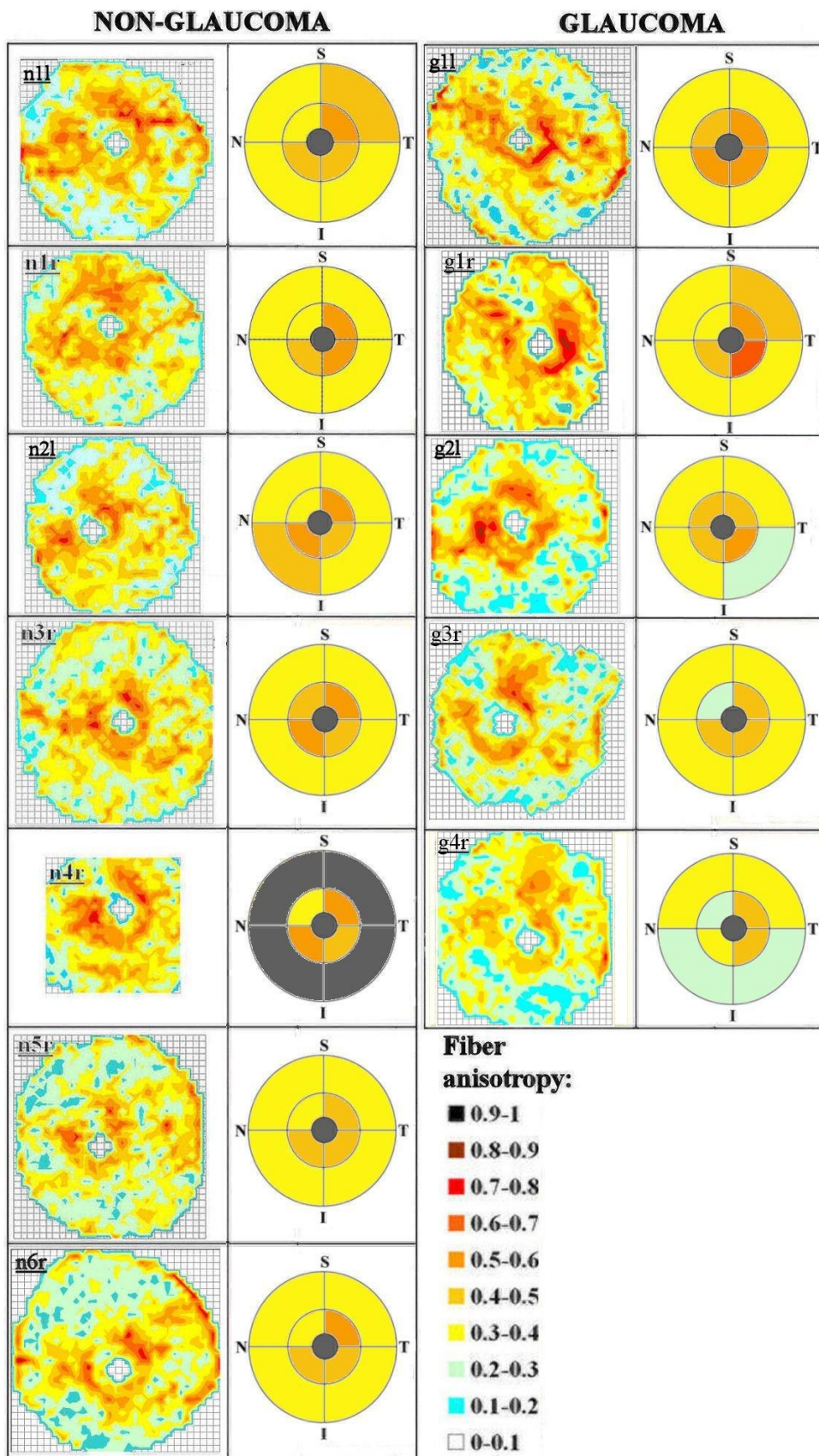
1

2 **Figure 4**



1

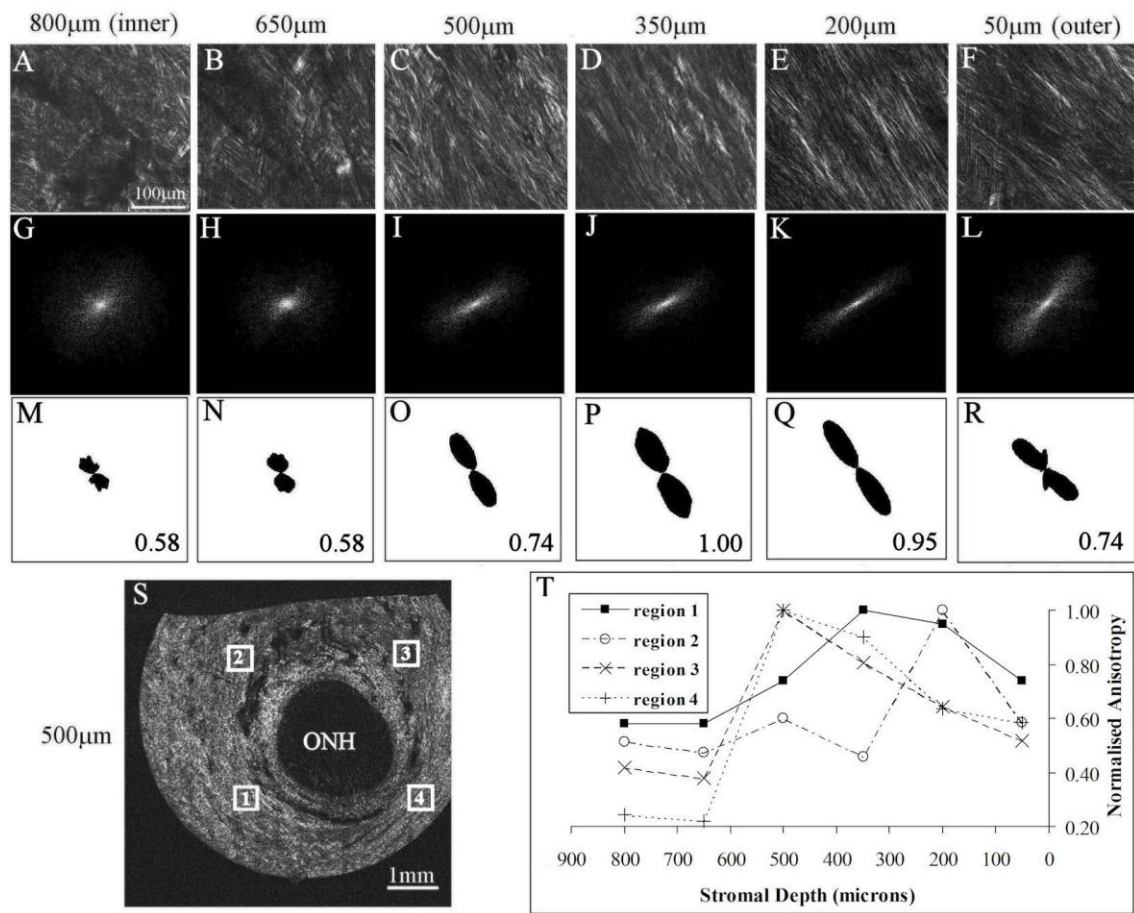
2 **Figure 5**



1

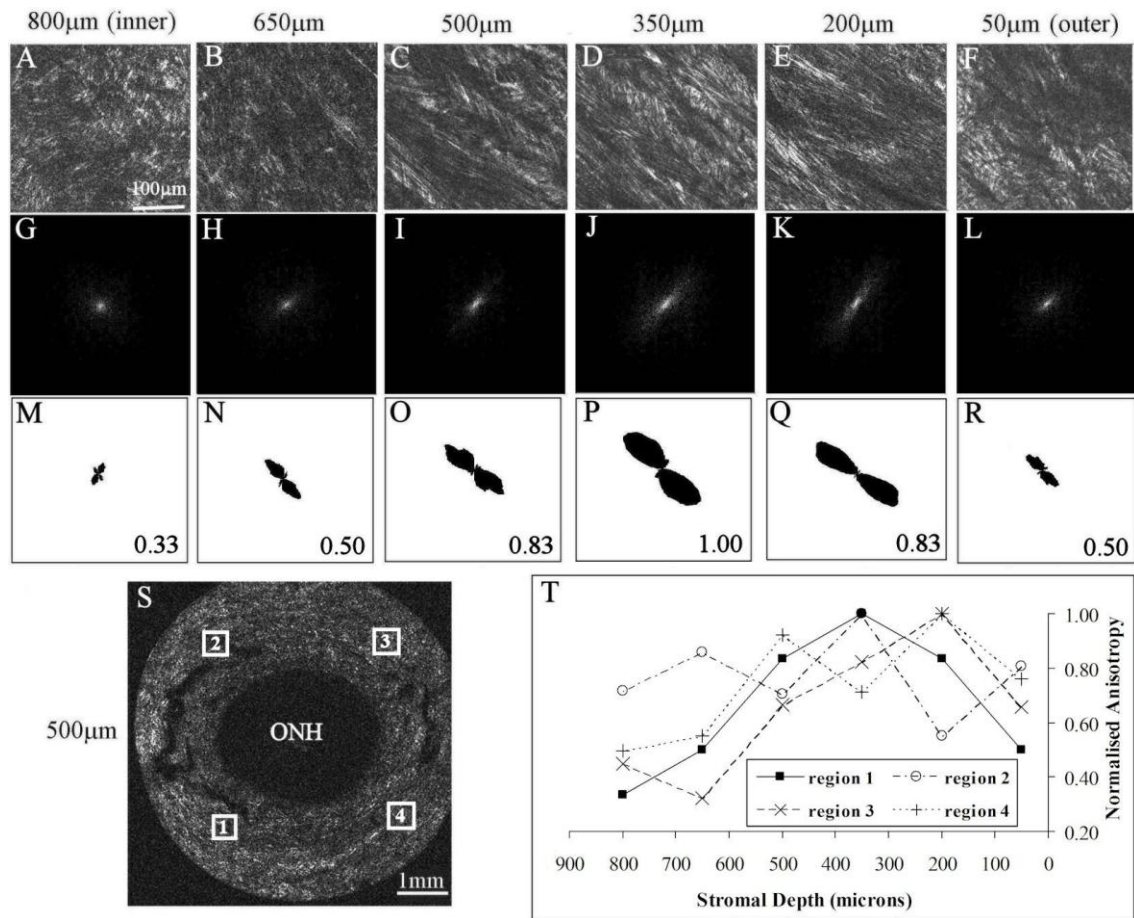
2 **Figure 6**

1



2

3 **Figure 7**



1

2 **Figure 8**

3

4

5

6

7

8

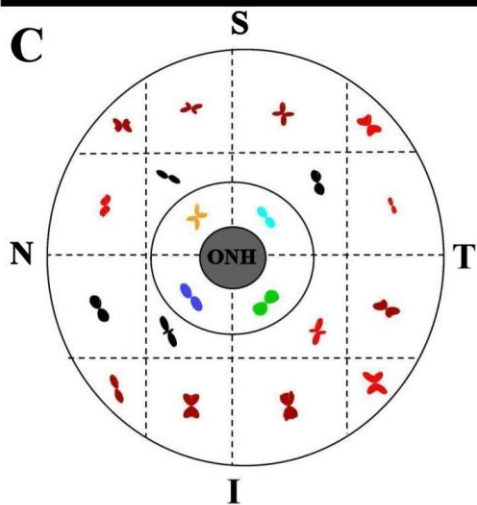
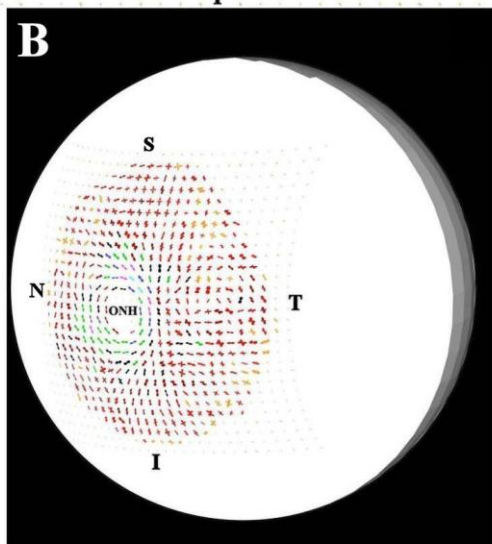
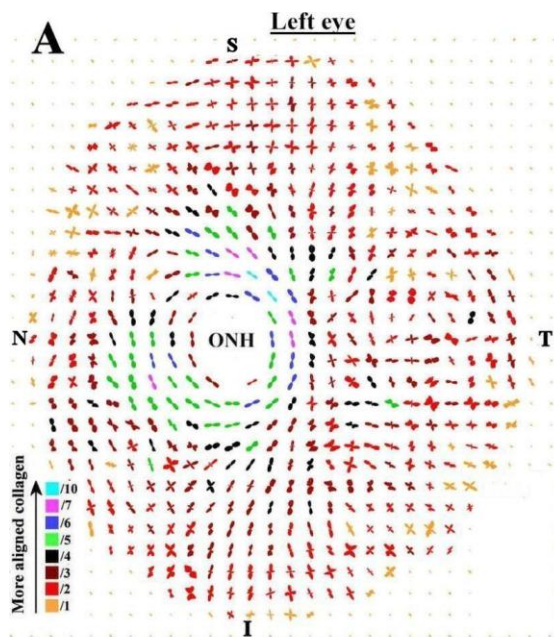
9

10

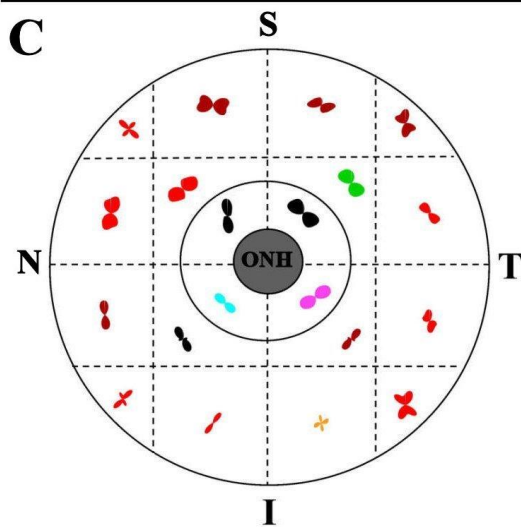
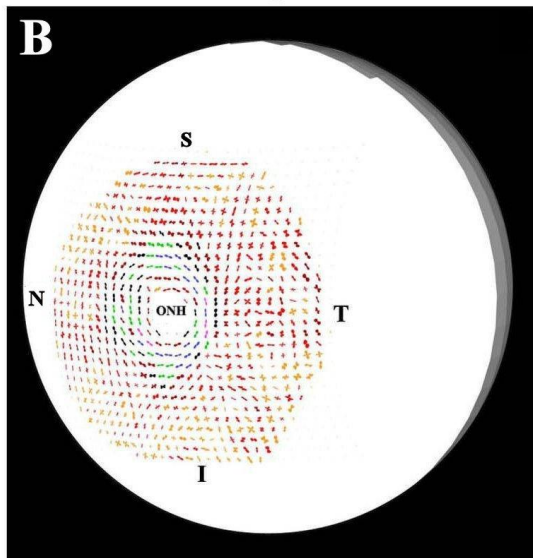
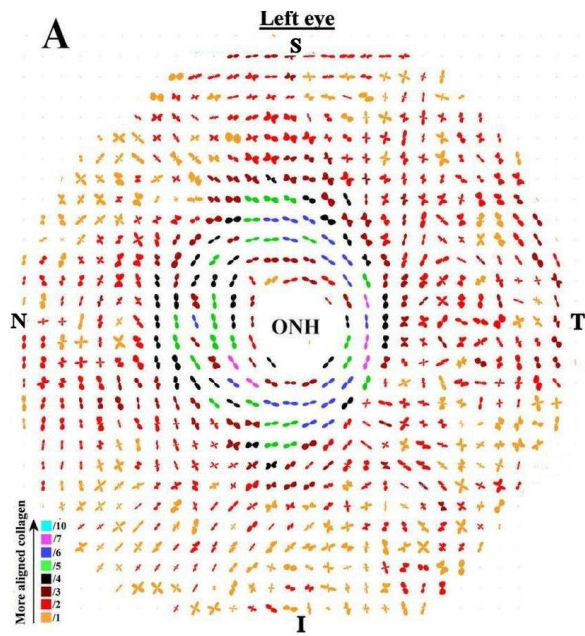
11

12

## 1 SUPPLEMENTARY MATERIAL



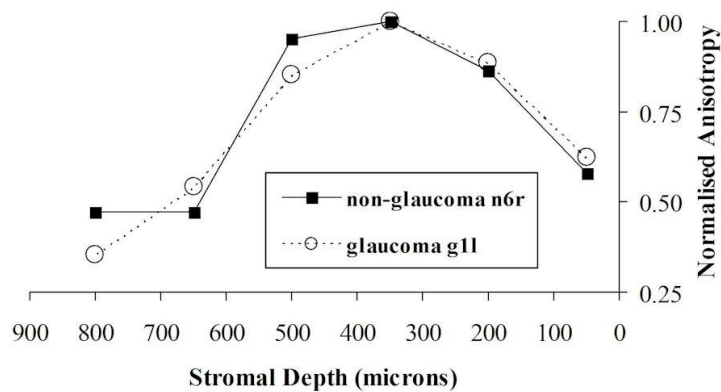
1 **Figure S1:**(A) Polar vector map of preferential collagen fiber orientation across a  
2 15mm diameter posterior scleral specimen (n21) from the left eye of a second non-  
3 glaucoma human donor, sampled at 0.5mm intervals, and viewed from the posterior  
4 side. The map has been mirror-flipped horizontally to enable direct comparison with  
5 right and left eyes in the main manuscript. (B) Polar vector plots mapped onto 3D  
6 posterior eye model. (C) Regional map showing average polar plots within the 4  
7 principal quadrants of the peripillary sclera and 16 regions of the mid-posterior tissue.



1 **Figure S2:** (A) Polar vector map of preferential collagen fiber orientation across a  
 2 15mm diameter posterior scleral specimen (g2l) from the left eye of a second glaucoma  
 3 human donor, sampled at 0.5mm intervals, and viewed from the posterior side. The map  
 4 has been mirror-flipped horizontally to enable direct comparison with right and left eyes  
 5 in the main manuscript. (B) Polar vector plots mapped onto 3D posterior eye model. (C)  
 6 Regional map showing average polar plots within the 4 principal quadrants of the  
 7 peripapillary sclera and 16 regions of the mid-posterior tissue.

8

9



10

11 **Figure S3:** Normalised fiber anisotropy as a function of stromal depth for non-  
 12 glaucoma specimen n6r and glaucoma specimen g11. The values displayed are averages  
 13 of four peripapillary scleral regions, corresponding to the locations shown in Figs. 7S  
 14 and 8S in the main manuscript.